Hindawi
Mathematical Problems in Engineering
Volume 2018, Article ID 4397548, 15 pages
https://doi.org/10.1155/2018/4397548

Research Article

Attitude Controller Design with State Constraints for Kinetic Kill Vehicle Based on Barrier Lyapunov Function

Tao Zhang, Jiong Li, Huaji Wang, ChuHan Xiao, and Wanqi Li

Air and Missile Defense College, Air Force Engineering University, Xi'an, Shaanxi 710051, China

Correspondence should be addressed to Tao Zhang; zhangtaov2016@163.com

Received 14 April 2018; Revised 22 July 2018; Accepted 9 August 2018; Published 5 September 2018

Academic Editor: Mihai Lungu

An adaptive attitude controller is designed based on Barrier Lyapunov Function (BLF) to meet the state constraints caused by side window detection. Firstly, the attitude controller is designed based on the BLF, but the stabilization function is complex and its time derivative will cause "differential explosion". Therefore, Finite-time-convergent Differentiator (FD) is used to estimate the first derivative of the stabilization function. If the tracking error is outside the BLF's convergence domain, BLF controller cannot guarantee the error global convergence. Sliding mode controller (SMC) is used to make the system's error converge to set domain, and then the BLF controller could be used to ensure that the output constraint is not violated. Uncertainties and unknown time-varying disturbances usually make the control precision worse and Nonlinear Disturbance Observer (NDO) is designed for estimation and compensation uncertainties and disturbances. The pseudo rate modulator (PSR) is used to shape the continuous control command to pulse or on-off signals to meet the requirements of the thruster. Numerical simulations show that the proposed method can achieve state constraints, pseudo-linear operation, and high accuracy.

1. Introduction

With the development of small-size propulsion systems, accurate sensors, and precision guidance systems, the kinetic kill vehicle (KKV) is now becoming both technically and economically feasible [1–3]. In order to satisfy the requirements of intercepting hypersonic targets in near space, KKV is generally flying at a high speed and equipped with infrared imaging seeker. However, when KKV is flying in near space with high speed, strong aerodynamic heating will seriously affect the seeker detection accuracy. To solve this problem, the seeker is usually mounted on the KKV's lateral side to avoid heat-intensive areas in front of the body. The installation and detection method of configuring the seeker on the lateral side of the missile is defined as side window detection [4, 5].

Side window detection will inevitably affect the field of view of seeker and in order to ensure that the target is always located in the field of view, the elevation angle q_ε^b and the azimuth angle q_β^b in body-LOS coordinate should be maintained in $[q_{\varepsilon\min}^b, q_{\varepsilon\max}^b]$ and $[q_{\beta\min}^b, q_{\beta\max}^b]$, and the system overshoot is within this range [6]. In the terminal guidance, the control system is a fast variable relative to the guidance system, so we mainly rely on the control system to ensure that the target is always in the field of view of the seeker. It is necessary to constrain the steady-state performance and dynamic performance of the attitude control system to the set domain. The above problem can be attributed to the stabilization of the nonlinear system with output constraints.

The current methods of controller design, such as sliding mode control [7–9], backstepping control [10, 11], and dynamic surface control [12, 13], are usually unable to design the dynamic performance of the controller. Control design for the constrained nonlinear system is commonly carried out using a two-step approach. After a closed-loop system design has been determined, often without explicitly considering state constraints, the dynamic behavior is investigated most often by simulation studies. Control design is usually based on mathematical models, which are subject to uncertainties and unknown time-varying disturbances. Therefore, any control design approach should systematically account for both state constraints and uncertainty.

Constraint-handling methods based on set invariance [14], model predictive control [15], override control [16, 17], and reference governors [18] are well established. However, these methods are essentially based on numerical calculations, and the calculations are more complicated.

More recently, the use of BLF has been proposed to realize the output and state constraints for strict feedback and output feedback nonlinear system. Ngo [19] constructs an arctangent and logarithmic barrier function as the control Lyapunov function for the Brunovsky standard system and realizes state constraints. The work in [20] presented control designs for strict feedback nonlinear systems with a constant output constraint and [21, 22] further extend the results to strict feedback nonlinear systems with time-varying output constraint. Tee [23] rigorously proved that the backstepping controller designed with symmetric BLF or asymmetric BLF can ensure the system output is bounded for a strict feedback nonlinear system. But this method requires the system to be in a small convergence domain and the output to be continuously differentiable, and this is usually not satisfied in the actual system. Tee [24] then proposed an improved method. If the initial state of the system is outside the convergence domain, it is necessary to reselect the BLF to make the system converge to the set domain. This method can guarantee the system converges to the set domain, but the initial state is difficult to obtain and system cannot realize the adaptive control. In addition, BLF-based control has been applied to practical systems, such as electrostatic oscillators [25], flexible crane system [26], and diesel engines [27].

Many controllers designed with nonlinear control theory are continuous and they cannot be directly applied to the attitude control system of KKV. To solve this problem, many pulse modulators have been proposed to convert continuous control variables into a pulse or on-off signals, such as pulse width modulation (PWM), pulse frequency modulation (PFM), and pulse width pulse frequency modulation (PWPF) [2, 28–30]. PWPF modulation method is widely used in aircraft attitude control systems with its good control performance. Reference [2] uses the PWPF modulator to shape the continuous control command to pulse or on-off signals to meet the requirements of the reaction thrusters and the methods to select the appropriate parameters are presented in detail. Reference [28] discusses the performance of PWPF modulators in terms of approximate linear space, fuel consumption, and thruster operating frequency for the attitude control. In [29], the variable dead-zone PWPF modulator was designed, and the stability was proved by using the description function method. The simulation results show the superiority of the algorithm in fuel consumption and control accuracy. Reference [30] proposes a nonlinear objective optimization function for the limitations of PWPF modulator parameters setting. The genetic algorithm is used to optimize the parameters of the PWPF regulator which considers the performance requirements of guidance systems such as linear work area requirements, miss distance, and fuel consumption of PWPF regulators. PWPF can output pulse instructions of different width and the static characteristics are not related to the parameters of the aircraft, but the PWPF modulator has the problem of phase lag which could cause instability of the system.

Motivated by the above discussions, to meet the state constraints caused by side window detection, an attempt is made to exploit Barrier Lyapunov Function to design the attitude controller. To break through the limitation that the initial error has to be in a small domain and the tracking error cannot guarantee global convergence, sliding mode control is used to make the tracking error converge to the set domain if the initial error is not in the set domain. What is more, BLF-based control relies on the accurate model and requires the output continuously differentiable, NDO is designed for estimation and compensation these uncertainties and disturbances, and FD is designed to estimate derivative. The special contributions of this paper are summarized as follows:

(1) This paper investigate a BLF for KKV to meet the state constraints and achieve satisfactory dynamic performance and stationary performance compared with the existing work [2, 11].

(2) To overcome the shortcoming which requires that the initial error has to be in a small domain, existing in the work [19, 23, 24], sliding mode control is used to make the tracking error converge to the set domain if the initial error is not in the set domain.

(3) The PSR modulator is used to transform the continuous control law into the pulse control law. The constant thrust control is realized and the phase lag problem of the PWPF modulator is overcome compared with the existing work [2, 28, 30].

2. Problem Formulation and Preliminaries

2.1. The Mathematical Model of KKV. KKV is small enough to ignore the elastic vibration and study as a rigid body. The nonlinear equations of dynamic and kinematic are formulated as [11]

$$\begin{aligned}
&J_x\dot{\omega}_x + \left(J_z - J_y\right)\omega_y\omega_z = M_x + d_x \\
&J_y\dot{\omega}_y + \left(J_x - J_z\right)\omega_z\omega_x = M_y + d_y \\
&J_z\dot{\omega}_z + \left(J_y - J_x\right)\omega_x\omega_y = M_z + d_z \\
&\dot{\gamma} = \omega_x - \tan\vartheta\left(\omega_y\cos\gamma - \omega_z\sin\gamma\right) \\
&\dot{\psi} = \frac{\left(\omega_y\cos\gamma - \omega_z\sin\gamma\right)}{\cos\vartheta} \\
&\dot{\vartheta} = \omega_y\sin\gamma + \omega_z\cos\gamma
\end{aligned} \tag{1}$$

where the rigid body states ω_x, ω_y, and ω_z represent roll angle velocity, yaw angle velocity, and pitch angle velocity, respectively. J_x, J_y, and J_z are the moment of inertia of each axis. M_x, M_y, and M_z are the control torque on the axes which are provided by the thrusters. d_x, d_y, and d_z are the total uncertainties of each channel.

KKV has no rudder and no wing, and attitude adjustment of the KKV is realized only by the attitude control system

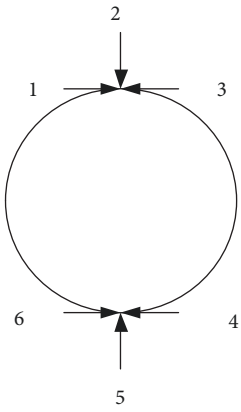

Figure 1: Attitude control thruster layout.

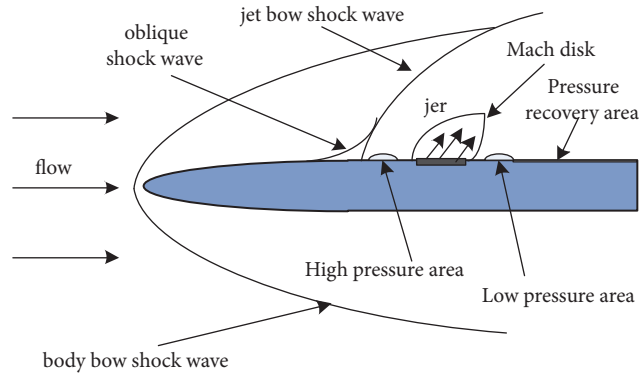

Figure 2: Jet Interaction Effects diagram.

installed at the rear of the body. KKV attitude is adjusted through 6 thrusters which are shown in Figure 1, with (2#+5#) thrusters controlling the pitch channel, (1#+6#) and (3#+4#) thrusters controlling the yaw channel, and (1#+4#) and (3#+6#) thrusters controlling the roll channel. The attitude control thrusters belong to the direct lateral jet propeller and it can only output the constant thrust.

The thrusts generated by the attitude control thrusters along each axis in the body coordinate are as follows:

$$\begin{aligned} F_{zx_1} &= 0 \\ F_{zy_1} &= F_{z5} - F_{z2} \\ F_{zz_1} &= F_{z1} + F_{z4} - F_{z3} - F_{z6} \end{aligned} \tag{2}$$

Then, we can obtain the control torque

$$\begin{aligned} M_{zx_1} &= \left(F_{z1} + F_{z4} - F_{z3} - F_{z6}\right) \cdot r \\ M_{zy_1} &= \left(F_{z1} + F_{z6} - F_{z3} - F_{z4}\right) \cdot l \\ M_{zz_1} &= \left(F_{z2} - F_{z5}\right) \cdot l \end{aligned} \tag{3}$$

where F_{zi} $(i = 1, \ldots, 6)$ is the thrust in a different direction; r is the radius of the body; l is the distance from the location of the thruster to the center of mass.

In the actual working process, in order to ensure the stability of the work and reduce the impact of thruster work on the system, the attitude control thruster usually works in pairs. Considering that the performance of the thruster is basically similar, (3) can be simplified to the following form:

$$\begin{aligned} M_{zx_1} &= 2F_z \cdot r\delta_{Fx} \\ M_{zy_1} &= 2F_z \cdot l\delta_{Fy} \\ M_{zz_1} &= F_z \cdot l\delta_{Fz} \end{aligned} \tag{4}$$

where F_z is the thrust of a single attitude control thruster and δ_{Fx}, δ_{Fy}, and δ_{Fz} determine whether to turn on.

When the attitude control thruster is turned on, the lateral jet flow interferes with the external flow field, forming a complicated flow field with a complicated structure. Jet flow produces a strong boundary layer separation, which causes oblique shock wave, split shock wave, bow shock wave, reattach shock wave, splitting nest, and secondary splitting nest in the flow field, and the expansion wave appears on both sides of the jet. There may be complex physical phenomena such as internal shock waves and Mach disk in the jet stream area. This phenomenon is called lateral jet flow disturbance effect. Typical lateral jet flow and external flow field interference phenomena are shown in Figure 2.

The disturbing flow field is very complex and has the characteristics of distributed parameters. Yet there is no accurate mathematical model to describe it. Almost all the references adopt thrust amplification factor K_T and torque amplification factor K_M to describe the forces and moments generated on the aircraft due to the side spray and the incoming flow interfere with each other. Its definition is as follows:

$$\begin{aligned} K_T &= \frac{\left(T_c + T_d\right)}{T_c} \\ K_M &= \frac{\left(M_c + M_d\right)}{M_c} \end{aligned} \tag{5}$$

Among them, T_d is the interference force caused by the jet, T_c is the static thrust on the ground, M_d is the disturbance torque caused by the jet, and M_c is the static moment of the thruster on the ground. The direct control force and torque are

$$\begin{aligned} T &= \left(T_c + T_d\right) = K_T T_c \\ M_T &= \left(M_c + M_d\right) = K_M M_c \end{aligned} \tag{6}$$

Therefore, considering the jet flow disturbance, the actual torque can be expressed as

$$\begin{aligned} M_{jx} &= M_{zx} \\ M_{jy} &= K_{My} M_{zy} + \Delta M_{jy} \\ M_{jz} &= K_{Mz} M_{zz} + \Delta M_{jz} \end{aligned} \tag{7}$$

where M_{jx}, M_{jy}, and M_{jz}, respectively, represent the components of each axis in the KKV body coordinate system under

consideration of the jet flow disturbances. ΔM_{jy} and ΔM_{jz} are the disturbance moments in the Oy_1 axis and Oz_1 axis.

Define $\mathbf{X}_1 = [\vartheta \ \psi \ \gamma]^T$, $\mathbf{X}_2 = [\omega_x \ \omega_y \ \omega_z]^T$ and $\mathbf{u} = [\delta_{Fx} \ \delta_{Fy} \ \delta_{Fz}]$, then (1) can be rewritten in a more compact form as

$$\begin{aligned} \dot{\mathbf{X}}_1 &= \mathbf{G}\mathbf{X}_2 \\ \mathbf{J}\dot{\mathbf{X}}_2 &= \mathbf{F} + \mathbf{L}\mathbf{u} + \mathbf{D}(t) \end{aligned} \tag{8}$$

where

$$\mathbf{G} = \begin{bmatrix} 0 & \sin\gamma & \cos\gamma \\ 0 & \dfrac{\cos\gamma}{\cos\vartheta} & -\dfrac{\sin\gamma}{\cos\vartheta} \\ 1 & -\tan\vartheta\cos\gamma & \tan\vartheta\sin\gamma \end{bmatrix}$$

$$\mathbf{J} = \begin{bmatrix} J_x & 0 & 0 \\ 0 & J_y & 0 \\ 0 & 0 & J_z \end{bmatrix},$$

$$\mathbf{F} = \begin{bmatrix} (J_z - J_y)\omega_y\omega_z \\ (J_x - J_z)\omega_z\omega_x \\ (J_y - J_x)\omega_x\omega_y \end{bmatrix} \tag{9}$$

$$\mathbf{L} = \begin{bmatrix} 2F_z \cdot r & 0 & 0 \\ 0 & 2K_{My}F_z \cdot l & 0 \\ 0 & 0 & K_{Mz}F_z \cdot l \end{bmatrix},$$

$$\mathbf{D}(t) = \begin{bmatrix} d_x \\ d_y + \Delta M_{jy} \\ d_z + \Delta M_{jz} \end{bmatrix}$$

When the KKV adjusts the attitude or orbit, thruster consumes fuel which leads to the change of the moment of inertia and the drift of the center of mass. It is described as follows:

$$\begin{aligned} \mathbf{J} &= \mathbf{J}_0 + \Delta\mathbf{J} \\ \mathbf{F} &= \mathbf{F}_0 + \Delta\mathbf{F} \\ \mathbf{L} &= \mathbf{L}_0 + \Delta\mathbf{L} \end{aligned} \tag{10}$$

where $\mathbf{J}_0$, $\mathbf{F}_0$, and $\mathbf{L}_0$ are the initial value of $\mathbf{J}$, $\mathbf{F}$, and $\mathbf{L}$ and $\Delta\mathbf{J}$, $\Delta\mathbf{F}$, and $\Delta\mathbf{L}$ are the variation of parameters which satisfy the following assumption.

Assumption 1. The disturbance moment satisfies the bounded condition and there is a bounded function $\xi(t)$ to let $\|\mathbf{D}(t)\| \leq \xi(t)$.

Assumption 2. The distance uncertainty of the attitude control torque satisfies the $\Delta l_i \leq l_{\theta i}$, where $l_{\theta i}$ $(i = r, l)$ are the arithmetic number.

Assumption 3. $\mathbf{J}_0^{-1}$ exists and there are the uncertain constants μ_1, μ_2, and μ_3 to satisfy

$$\begin{aligned} \|\mathbf{J}_0\| &\leq \mu_1 < \infty, \\ \left\|\mathbf{J}^{-1}\right\| &\leq \mu_2 < \infty, \\ \|\Delta\mathbf{J}\| &\leq \mu_3 < \infty. \end{aligned} \tag{11}$$

Substituting (10) into (8)

$$(\mathbf{J}_0 + \Delta\mathbf{J})\dot{\mathbf{X}}_2 = (\mathbf{F}_0 + \Delta\mathbf{F}) + (\mathbf{L}_0 + \Delta\mathbf{L})\mathbf{u} + \mathbf{D}(t) \tag{12}$$

Then the problem has the following state-space representation:

$$\begin{aligned} \dot{\mathbf{X}}_1 &= \mathbf{G}\mathbf{X}_2 \\ \dot{\mathbf{X}}_2 &= \mathbf{J}_0^{-1}\mathbf{F}_0 + \mathbf{J}_0^{-1}\mathbf{L}_0\mathbf{u} + \mathbf{H}(t) \end{aligned} \tag{13}$$

where

$$\begin{aligned} \mathbf{H}(t) = {} & \mathbf{J}_0^{-1}(\Delta\mathbf{F} + \Delta\mathbf{L}\mathbf{u} + \mathbf{D}(t)) \\ & + \Delta\widetilde{\mathbf{J}}[\mathbf{F}_0 + \Delta\mathbf{F} + \mathbf{L}_0\mathbf{u} + \Delta\mathbf{L}\mathbf{u} + \mathbf{D}(t)] \end{aligned} \tag{14}$$

From (13), we can know that the mathematical model of KKV attitude system is strict feedback form which includes state constraints and uncertainty.

2.2. Finite-Time-Convergent Differentiator. Without loss of generality, we consider the following uncertain dynamic system:

$$\begin{aligned} \dot{x}_1 &= x_2 \\ \dot{x}_2 &= x_3 \\ &\vdots \\ \dot{x}_{n-1} &= x_n \\ \dot{x}_n &= f(x_1, x_2, \ldots, x_n) \end{aligned} \tag{15}$$

where $x_1, x_2, \ldots, x_n \in \mathbf{R}$ are the state variables, $f_A(\bullet)$ is a continuous function, and $f(0, \ldots, 0) = 0$.

Lemma 4 (see [31]). *For system (16)*

$$\begin{aligned} \dot{z}_1 &= z_2 \\ \dot{z}_2 &= F(z_1(t), z_2(t)) \end{aligned} \tag{16}$$

where $z_1 \in R$, $z_2 \in R$, if system (16) satisfies $z_1(t) \longrightarrow 0$, $z_2(t) \longrightarrow 0 (t \longrightarrow \infty)$. For any an arbitrary bounded function $v(t)$ and a constant $T > 0$, the solution of the system

$$\begin{aligned} \dot{x}_1 &= x_2 \\ \dot{x}_2 &= R^2 F\left(x_1(t) - v(t), \frac{x_2}{R}\right) \end{aligned} \tag{17}$$

satisfies

$$\lim_{R\longrightarrow\infty} \int_0^T |x_1 - v(t)|\, dt = 0 \tag{18}$$

Remark 5. $x_1(t)$ averagely converges to the input signal $v(t)$ and $x_2(t)$ converges to the generalized derivative of $v(t)$. In (17), $R > 0$ is a design parameter.

According to Lemma 4, a simple FD is presented as follows:

$$\begin{aligned}
\dot{\varsigma}_1 &= \varsigma_2 \\
\dot{\varsigma}_2 &= \varsigma_3 \\
&\vdots \\
\dot{\varsigma}_{n-1} &= \varsigma_n \\
\dot{\varsigma}_n &= R^n \left[-a_1 \tanh\left(\varsigma_1 - v\left(t\right)\right) - a_2 \tanh\left(\frac{\varsigma_2}{R}\right) - \right] \\
&\quad \cdots - a_n \tanh\left(\frac{\varsigma_n}{R^{n-1}}\right)
\end{aligned} \tag{19}$$

where R, a_i $(i = 1, 2, \ldots, n) \in \mathbf{R}^+$ is design parameter and there are $\phi > 0$ and $\iota\phi > n$ which satisfies

$$\varsigma_i - v^{(i-1)}\left(t\right) = O\left(\left(\frac{1}{R}\right)^{\iota\phi - i + 1}\right), \quad i = 1, 2, \cdots, n \tag{20}$$

where $O((1/R)^{\iota\phi-i+1})$ is the $(1/R)^{\iota\phi-i+1}$ order error of $v^{(i-1)}(t)$, $\phi = (1-\vartheta)/\vartheta$, $\vartheta \in (0, \min\{\iota/(\iota+n), 1/2\})$, $n \geq 2$.

2.3. Nonlinear Disturbance Observers. In this section, a new NDO is designed based on FD. Without loss of generality, we consider the following uncertain dynamic system:

$$\dot{v} = F\left(v\right) + G\left(v\right)u + d \tag{21}$$

where $v \in R$ and $u \in R$ are the state and control input respectively. $F(v)$ and G$(v) \neq 0$ are the continuous function. $d \in R$ denotes the disturbance.

Theorem 6. *The following new NDO is designed for the uncertain system (21):*

$$\begin{aligned}
\dot{\widehat{v}} &= F\left(v\right) + G\left(v\right)u + \widehat{d} \\
\dot{\widehat{d}} &= R^2 \left[-a_1 \tanh\left(\widehat{v} - v\right) - a_2 \tanh\left(\frac{\widehat{d}}{R}\right) \right]
\end{aligned} \tag{22}$$

where v is the estimated value of $\widehat{v}$ and d is the estimated value of $\widehat{d}$; if $R \longrightarrow +\infty$, then

$$\begin{aligned}
\widehat{v} - v &= O\left(\left(\frac{1}{R}\right)^{\iota\phi}\right) \\
\widehat{d} - d &= O\left(\left(\frac{1}{R}\right)^{\iota\phi - 1}\right)
\end{aligned} \tag{23}$$

Proof. There are two main steps in the proof.

Step 1

If $\widehat{v} - v = 0$, then compared to the first equation of (22) and (23), we can obtain that $\widehat{d} - d = 0$. Theorem 6 holds obviously.

Step 2

If $\widehat{v} - v \neq 0$, when $R \longrightarrow +\infty$, $\tanh(\widehat{d}/R) \longrightarrow 0$, we can obtain

$$-a_1 \tanh\left(\widehat{v} - v\right) - a_2 \tanh\left(\frac{\widehat{d}}{R}\right) \neq 0 \tag{24}$$

Then

$$\left|\dot{\widehat{d}}\right| = R^2 \left| -a_1 \tanh\left(\widehat{v} - v\right) - a_2 \tanh\left(\frac{\widehat{d}}{R}\right) \right| \longrightarrow +\infty \tag{25}$$

Compared to v and $F(v) + G(v)u$, $\widehat{d}$ is fast variable. According to [31], we obtain

$$\begin{aligned}
\lim_{R \longrightarrow +\infty} \frac{\mathrm{d}\left[F\left(v\right) + G\left(v\right)u + \widehat{d}\right]}{\mathrm{d}t} &= \dot{\widehat{d}} \\
\lim_{R \longrightarrow +\infty} \frac{F\left(v\right) + G\left(v\right)u + \widehat{d}}{R} &= \frac{\widehat{d}}{R}
\end{aligned} \tag{26}$$

If n=2, then (19) is

$$\begin{aligned}
\dot{\varsigma}_1 &= \varsigma_2 \\
\dot{\varsigma}_2 &= R^2 \left[-a_1 \tanh\left(\varsigma_1 - v\left(t\right)\right) - a_2 \tanh\left(\frac{\varsigma_2}{R}\right) \right]
\end{aligned} \tag{27}$$

Substituting $F(v) + G(v)u + \widehat{d}$ into (27) and combining with (26), Theorem 6 holds obviously. □

3. Attitude Controller Design and Realization

Throughout this paper, we denote by $\mathbb{R}_+$ the set of nonnegative real numbers, $\| \bullet \|$ the Euclidean vector norm in $\mathbb{R}^m$, and $\lambda_{\max}(\bullet)$ and $\lambda_{\min}(\bullet)$ the maximum and minimum eigenvalues of $\bullet$, respectively. For illustration purpose, we consider a class of second-order strict feedback systems and outline the control design based on a BLF to ensure that the output constraint is not violated. Consider the system

$$\begin{aligned}
\dot{x}_1 &= f_1\left(x_1\right) + g_1\left(x_1\right)x_2 + d_1 \\
\dot{x}_2 &= f_2\left(x_1, x_2\right) + g_2\left(x_1, x_2\right)u + d_2 \\
y &= x_1
\end{aligned} \tag{28}$$

where $f_1(x_1)$, $f_2(x_1, x_2)$, $g_1(x_1)$, and $g_2(x_1, x_2)$ are smooth functions, $u \in \mathbb{R}$ is the control input, and $x_1, x_2 \in \mathbb{R}$ are the states, with y required to satisfy $|y| < k_{c1}$, $\forall t \geq 0$, with k_{c1} being a positive constant.

Assumption 7. The function $g_i(x_i)$, $i = 1, 2, \ldots, n$, is known, and there exists a positive constant g_0 such that $0 < g_0 \leq |g_i(x_i)|$ for $|x_1| < k_{c_i}$. Without loss of generality, we further assume that $g_i(x_i)$ are all positive for $|x_1| < k_{c_i}$.

Lemma 8. *For any positive constants k_{a_1} and k_{b_1}, let $\mathbb{Z}_1 := \{z_1 \in \mathbb{R} : -k_{a_1} < z_1 < k_{b_1}\} \subset \mathbb{R}$ and $\mathbb{N} := \mathbb{R}^l \times \mathbb{Z}_1 \subset \mathbb{R}^{l+1}$ be open sets. Consider the system*

$$\dot{\eta} = h\left(t, \eta\right) \tag{29}$$

where $\eta := [w, z_1]^T \in \mathbb{N}$ *and* $h : \mathbb{R}_+ \times \mathbb{N} \longrightarrow \mathbb{R}^{l+1}$ *is piecewise continuous in* t *and locally Lipchitz in* z*, uniform in* t*, on* $\mathbb{R}_+ \times \mathbb{N}$*. Suppose that there exist functions* $U : \mathbb{R}^l \longrightarrow \mathbb{R}_+$ *and* $V_1 : \mathbb{Z}_1 \longrightarrow \mathbb{R}_+$*, continuously differentiable and positive definite in their respective domains, such that*

$$V_1(z_1) \longrightarrow \infty \quad \text{as } z_1 \longrightarrow -k_{a_1} \text{ or } z_1 \longrightarrow k_{b_1} \tag{30}$$

$$\gamma_1(\|w\|) \le U(w) \le \gamma_2(\|w\|) \tag{31}$$

where γ_1 *and* γ_2 *are class* K_∞ *functions. Let* $V(\eta) := V_1(z_1) + U(w)$*, and* $z_1(0)$ *belong to the set* $z_1 \in (-k_{a_1}, k_{b_1})$*. If the inequality holds*

$$\dot{V} = \frac{\partial V}{\partial \eta} h \le 0 \tag{32}$$

then $z_1(t)$ *remains in the open set* $z_1 \in (-k_{a_1}, k_{b_1})\ \forall t \in [0, \infty)$.

Remark 9. In Lemma 8, we split the state space into z_1 and w, where z_1 is the state to be constrained and w is the free states. The constrained state z_1 requires the barrier function $V_1$to prevent it from reaching the limits $-k_{a_1}$ and k_{b_1}, while the free states may involve quadratic functions.

For system (28), we employ backstepping design as follows.

Step 1. Let $z_1 = y_1 - y_d$, $z_2 = x_2 - \alpha_1$, where y_d is the desired value, and α_1 is a stabilizing function to be designed. Chose the following symmetric BLF candidate:

$$V_1 = \frac{1}{2} \log \frac{k_{b_1}^2}{k_{b_1}^2 - z_1^2} \tag{33}$$

where $\log(\bullet)$ denotes the natural logarithm of $\bullet$ and $k_{b_1} = k_{c_1} - y_d$ denotes the constraint on z_1. We require $|z_1| < k_{b_1}$. It can be shown that V_1 is positive definite and thus a valid Lyapunov function candidate. The derivative of V_1 is given by

$$\dot{V}_1 = \frac{z_1 \dot{z}_1}{k_{b_1}^2 - z_1^2} = \frac{z_1 \left(f_1 + g_1 (z_2 + \alpha_1) + d_1 - \dot{y}_d\right)}{k_{b_1}^2 - z_1^2} \tag{34}$$

Design the stabilizing function α_1 as

$$\alpha_1 = \frac{1}{g} \left(-f_1 - \left(k_{b_1}^2 - z_1^2\right) k_1 z_1 - d_1 + \dot{y}_d\right) \tag{35}$$

where $k_1 > 0$ is a constant. Substituting (35) into (34) yields

$$\dot{V}_1 = -k_1 z_1^2 + \frac{g_1 z_1 z_2}{k_{b_1}^2 - z_1^2} \tag{36}$$

where the coupling term $g_1 z_1 z_2 / (k_{b_1}^2 - z_1^2)$ is cancelled in the subsequent step.

Step 2. Since x_2 does not need to be constrained, we choose a Lyapunov function candidate by augmenting V_1 with a quadratic function:

$$V_2 = V_1 + \frac{1}{2} z_2^2 \tag{37}$$

The time derivative of V_2 is given by

$$\dot{V}_2 = -k_1 z_1^2 + \frac{g_1 z_1 z_2}{k_{b_1}^2 - z_1^2} + z_2 \left(f_2 + g_2 u + d_2 - \dot{\alpha}_1\right) \tag{38}$$

The control law is designed as

$$u_{BLF} = \frac{1}{g_2} \left(-f_2 + d_2 + \dot{\alpha}_1 - k_2 z_2 - \frac{g_1 z_1}{k_{b_1}^2 - z_1^2}\right) \tag{39}$$

where $k_2 > 0$ is constant and the last term on the right-hand side is to cancel the residual coupling term $g_1 z_1 z_2 / (k_{b_1}^2 - z_1^2)$ from the first step. Substituting (39) into (38) yields $\dot{V}_2 = -\sum_{i=1}^{2} k_i z_i^2$. From (39), there is a concern of $u(t)$ becoming unbounded whenever $|z_1(t)| = k_{b_1}$. However, we have established that, in the closed loop, the error signal $|z_1(t)|$ never reaches $k_{b_1} \forall t \ge 0$. As a result, the control $u(t)$ will not become unbounded because of the presence of terms comprising $(k_{b_1}^2 - z_1^2(t))$ in the denominator.

According to Lemma 8, we have $|z_1(t)| < k_{b_1}\ \forall t > 0$ and the output constraint will never be violated. Provide that the initial conditions satisfy

$$\left|z_1(0)\right| < k_{b_1} \tag{40}$$

However, we cannot always guarantee $|z_1(t)| < k_{b_1}\ \forall t > 0$ if the initial conditions $|z_1(0)| > k_{b_1}$. Next, SMC is used to make the initial error sliding to the set domain if the initial error is not in the set domain.

Firstly, transform system (28) as follows:

$$\dot{x} = f(x) + g(x) u \tag{41}$$

where $f(x) = [f_1(x_1) + g_1(x_1)x_2, \ldots, f_{n-1}(x_{n-1}) + g_{n-1}(x_{n-1})x_n, f_n(x_n)]^T$, $g(x) = [0, 0, \ldots, g_n(x_n)]^T$.

Then, the sliding mode surface is selected as follows:

$$s(x) = cx = c_1 x_1 + c_2 x_2 + \cdots + c_n x_n \tag{42}$$

The derivative of $s(x)$ is given by

$$\dot{s}(x) = c\left(f(x) + g(x) u_{SMC}\right) = -\varepsilon \operatorname{sign}(s) - ks \tag{43}$$

If $cg(x)$ is reversible, we can obtain the control law

$$u_{SMC} = \left(cg(x)\right)^{-1} \left(-cf(x) - \varepsilon \operatorname{sign}(s) - ks\right) \tag{44}$$

Choose the following Lyapunov function candidate:

$$V_0 = \frac{1}{2} s^2 \tag{45}$$

Differentiating V_0 and combining (42)–(44), we can obtain

$$\dot{V}_0 = s\dot{s} = -\varepsilon |s| - ks^2 \le 0 \tag{46}$$

The system gradually converges to the desired point.

Combining the SMC and BLF backstepping control, the global convergence output constraint robust control law is designed as follows:

$$u = pu_{BLF} + (1 - p)\, u_{SMC} \tag{47}$$

where

$$p = \begin{cases} 1, & |z_1| < k_{b_1} \\ 0, & |z_1| \geq k_{b_1} \end{cases} \tag{48}$$

Controller combining the SMC and BLF backstepping control can guarantee the error global convergence.

From KKV's mathematical model, we can see that system (13) satisfies the strict feedback form. Next, the method combining the sliding mode control and BLF backstepping control will be applied to design KKV controller with state constraints.

Define

$$\begin{aligned} \mathbf{Z}_1 &= \mathbf{X}_1 - \mathbf{X}_d \\ \mathbf{Z}_2 &= \mathbf{X}_2 - \boldsymbol{\beta}_1 \end{aligned} \tag{49}$$

where $\mathbf{Z}_1 \in (-\mathbf{K}_{b_1}, \mathbf{K}_{b_1})$, $\mathbf{K}_{b_1} = [\vartheta_{b_1}, \varphi_{b_1}, \gamma_{b_1}] = [1^\circ, 1^\circ, 1^\circ]^T$. Therefore, the domain of $\mathbf{Z}_1$ is $([-1^\circ, 1^\circ], [-1^\circ, 1^\circ], [-1^\circ, 1^\circ])^T$. Then we can get the stabilizing function $\boldsymbol{\beta}_1$:

$$\boldsymbol{\beta}_1 = \frac{1}{\mathbf{G}_0}\left(-\left(\mathbf{K}_{b_1}^2 - \mathbf{Z}_1^2\right)\mathbf{K}_1\mathbf{Z}_1 + \dot{\mathbf{X}}_{1ref}\right) \tag{50}$$

The BLF controller is designed as

$$\mathbf{u}_{BLF} = \frac{1}{\mathbf{J}_0^{-1}\mathbf{L}_0}\left(-\mathbf{J}_0^{-1}\mathbf{F}_0 - \mathbf{H}(t) + \dot{\boldsymbol{\beta}}_1 - \mathbf{K}_2\mathbf{Z}_2 - \frac{\mathbf{G}\mathbf{Z}_1}{\mathbf{K}_{b_1}^2 - \mathbf{Z}_1^2}\right) \tag{51}$$

From (50)-(51), we can know that the stabilizing function $\boldsymbol{\beta}_1$ is complex and the first derivative of $\boldsymbol{\beta}_1$ will bring about "differential explosion" and affect the efficiency of computer solution. The FD is used to solve this problem. The unknown total disturbance appears in the actual control; [32] points out that the maximum disturbance torque can reach 50 percent of the control torque. Under the condition of such a large disturbance moment, it is difficult to solve this problem only by the robustness of the system. If we do not carry out active control, it will reduce the precision of attitude control and even cause the instability of the system. Therefore, NDO is used to estimate and compensate the unknown disturbance.

Therefore, the first differential value of stabilizing function can be obtained as follows:

$$\begin{aligned} \dot{\boldsymbol{\varsigma}}_1 &= \boldsymbol{\varsigma}_2 \\ \dot{\boldsymbol{\varsigma}}_2 &= \mathbf{R}_1{}^2\left[-\mathbf{A}_1 \tanh(\boldsymbol{\varsigma}_1 - \boldsymbol{\beta}_1) - \mathbf{A}_2 \tanh\left(\frac{\boldsymbol{\varsigma}_2}{\mathbf{R}}\right)\right] \end{aligned} \tag{52}$$

where $\mathbf{A}_1 = \mathrm{diag}(a_{11}, a_{12}, a_{13})$, $a_{1i} > 0$, $i = 1, 2, 3$, $\mathbf{A}_2 = \mathrm{diag}(a_{21}, a_{22}, a_{23})$, $a_{2i} > 0$, $i = 1, 2, 3$, R_1 are the design parameters and $\boldsymbol{\varsigma}_2$ is the estimated value of $\dot{\boldsymbol{\beta}}$.

For system (13), the following NDO is designed:

$$\begin{aligned} \dot{\widehat{\mathbf{X}}}_2 &= \mathbf{F}(v) + \mathbf{G}(v)\,\mathbf{u} + \widehat{\mathbf{H}}(t) \\ \dot{\widehat{\mathbf{H}}}(t) &= \mathbf{R}_2{}^2\left[-\mathbf{A}_3 \tanh\left(\widehat{\mathbf{X}}_2 - \mathbf{X}_2\right) - \mathbf{A}_4 \tanh\left(\frac{\widehat{\mathbf{d}}}{\mathbf{R}}\right)\right] \end{aligned} \tag{53}$$

where $\mathbf{A}_3 = \mathrm{diag}(a_{31}, a_{32}, a_{33})$, $a_{3i} > 0$, $i = 1, 2, 3$, $\mathbf{A}_4 = \mathrm{diag}(a_{41}, a_{42}, a_{43})$, $a_{4i} > 0$, $i = 1, 2, 3$, $\mathbf{R}_2$ are design parameters.

Transform system (13) to a simple form as follows:

$$\dot{\mathbf{x}} = \mathbf{f}(x) + \mathbf{g}(x)\,\mathbf{u} \tag{54}$$

where $\mathbf{f}(\mathbf{x}) = [\mathbf{G}\mathbf{X}_2, \mathbf{J}_0^{-1}\mathbf{F}_0]$, $\mathbf{g}(\mathbf{x}) = [0, \mathbf{J}_0^{-1}\mathbf{L}_0]$.

Choose the following sliding mode surface:

$$s(x) = cx = c_1x_1 + c_2x_2 \tag{55}$$

Then, we can obtain SMC as

$$u_{SMC} = (cg(x))^{-1}(-cf(x) - \varepsilon\,\mathrm{sign}(s) - Ks) \tag{56}$$

Combining the SMC and BLF backstepping controller, the global convergence output constraint robust controller is designed as follows:

$$\mathbf{u} = \mathbf{p}\mathbf{u}_{BLF} + (1 - \mathbf{p})\,\mathbf{u}_{SMC} \tag{57}$$

where

$$\mathbf{p} = \begin{cases} \mathrm{diag}(1, 1, 1), & |x_1| \leq k_{b_1} \\ \mathrm{diag}(0, 0, 0), & |x_1| > k_{b_1} \end{cases} \tag{58}$$

Theorem 10. *Consider the closed-loop system consisting of plant (13) with control laws (57), FD (52), and NDO (53). The all the signals involved are uniformly ultimately bounded.*

Proof. Proof can be divided into two steps.

Step 1

When $|\mathbf{Z}_1| > \mathbf{K}_{b_1}$, mainly for SMC at work. From (46), we can know the system is stable.

Step 2

When $|\mathbf{Z}_1| \leq \mathbf{K}_{b_1}$, mainly for BLF backstepping controller at work.

Define the estimation errors of NDO and FD is

$$\begin{aligned} \widetilde{\mathbf{H}} &= \widehat{\mathbf{H}}(t) - \mathbf{H}(t) \\ \tilde{\boldsymbol{\beta}} &= \hat{\boldsymbol{\beta}} - \dot{\boldsymbol{\beta}} \end{aligned} \tag{59}$$

Choose the following Lyapunov function candidate:

$$\mathbf{W}_0 = \frac{1}{2}\log\frac{\mathbf{K}_{b_1}^2}{\mathbf{K}_{b_1}^2 + \mathbf{Z}_1^2} + \frac{1}{2}\mathbf{Z}_2^2 \tag{60}$$

Differentiating W_0 and combining (59)-(60), we can obtain

$$\dot{\mathbf{W}}_0 = -\mathbf{K}_1\mathbf{Z}_1^2 - \mathbf{K}_2\mathbf{Z}_2^2 - \mathbf{Z}_2\widetilde{\mathbf{H}} - \mathbf{Z}_2\hat{\boldsymbol{\beta}}_1 \tag{61}$$

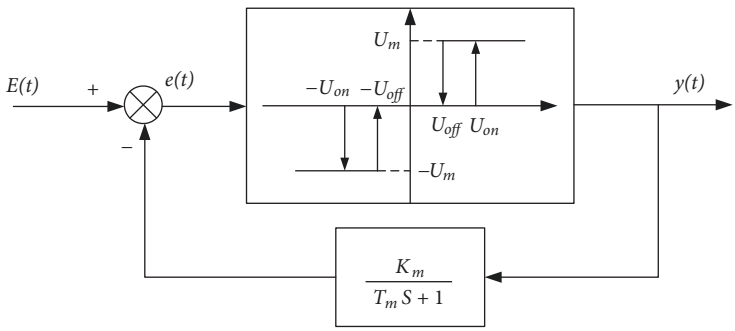

Figure 3: PSR modulator diagram.

Note that

$$\mathbf{Z}_2\widetilde{\mathbf{H}} \le \frac{\mathbf{Z}_2^2}{2} + \frac{\widetilde{\mathbf{H}}^2}{2}$$
$$\mathbf{Z}_2\hat{\boldsymbol{\beta}}_1 \le \frac{\mathbf{Z}_2^2}{2} + \frac{\hat{\boldsymbol{\beta}}_1^2}{2} \tag{62}$$

Substituting (61) into (62), the following inequality holds:

$$\dot{\mathbf{W}}_0 \le -\left(\mathbf{K}_1 + \frac{1}{2}\right)\mathbf{Z}_1^2 - \left(\mathbf{K}_2 + \frac{1}{2}\right)\mathbf{Z}_2^2 - \frac{\widetilde{\mathbf{H}}^2}{2} - \frac{\dot{\hat{\boldsymbol{\beta}}}_1^2}{2} \tag{63}$$

Therefore these tracking errors Z_1 and Z_2 are semiglobally uniformly bounded. By choosing the appropriate design parameters K_i $(i = 1, 2)$, these errors can be sufficiently small. This completes the proof. □

From (57), we can know that the control command is continuous type and cannot meet the pulse thruster requirement. Next, PSR modulator will be introduced to shape the continuous control command to pulse or on-off signals. The structure of the PSR modulator is similar to the PWPF modulator except that the position of the first-order inertial link is different. The PWPF first-order inertial link is located on the forward channel while the PSR modulator is located on the feedback channel. The schematic of the PSR modulator is shown in Figure 3.

When Schmitt trigger input $E(t)$ is greater than the start threshold, a fixed value of 1 is output. Modulator input $E(t)$ is exponentially decayed to subtract new $e(t)$. The output of the modulator is always 1 before $e(t)$ decrease to the shutdown threshold. The output of the modulator is 0 when the trigger input is less than the start-up threshold or after $e(t)$ decrease in the shutdown threshold. Similarly, when the input is negative, the modulator outputs 0 or −1 (negative sign means the modulator is reversed).

When the Schmitt trigger is on

$$e(t) = K_m(E - u_m)\left(1 - e^{-t_1/T_m}\right) + u_{on}e^{-t_1/T_m} \qquad 0 \le t_1 \le T_{on} \tag{64}$$

When the Schmitt trigger is off

$$e(t) = K_m(E - u_m)\left(1 - e^{-t_2/T_m}\right) + u_{off}e^{-t_2/T_m} \qquad 0 \le t_2 \le T_{off} \tag{65}$$

Then we can get the output pulse width

$$T_{on} = -T_m \ln\left[1 - \frac{h}{K_m u_m - (E - u_{on})}\right] \tag{66}$$

Schmitt trigger off time in one cycle is

$$T_{off} = -T_m \ln\left[1 - \frac{h}{K_m u_m - (E - u_{on})}\right] \tag{67}$$

Switching frequency is

$$f = \frac{1}{T_{on} + T_{off}} \tag{68}$$

Minimum pulse width is

$$\Delta \approx \frac{hT_m}{K_m} \tag{69}$$

The PSR pulse modulator not only has the same advantages which are similar to PWPF, with its static characteristics are also independent of the parameters of the aircraft, the output pulse is related to the error amplitude and error speed. It also provides phase advance performance compared to the PWPF.

4. Simulation Results

In this section, four kinds of simulation are established to verify the performance of the proposed method under the condition of strong disturbance. The control strategy for KKV with side window detection is to adjust the pitch angle and yaw angle to track the desired pitch angle and yaw angle accurately and keep the rolling angle stability to ensure the detecting field of view. The initial parameters and disturbance are listed in Table 1, the simulation parameters perturbation are listed in Table 2, and the simulation paremeters of FD and NDO are listed in Table 3.

Table 1: Simulation initial parameters.

parameter	parameter perturbation
J_{x0}	0.4
J_{y0}	0.4
J_{z0}	0.4
l	0.5
r	0.16
d_x	$3^\circ \sin((\pi/2)\,t)$
d_y	$3^\circ \sin((\pi/2)\,t)$
d_z	$3^\circ \sin((\pi/2)\,t)$

Table 2: Simulation parameters perturbation.

parameter	parameter perturbation
ΔJ_x	$J_{x0} \times 20\% \sin(t)$
ΔJ_y	$J_{x0} \times 30\% \sin(t)$
ΔJ_z	$J_{z0} \times 10\% \sin(t)$
Δl	$l \times 20\% \sin(t)$
Δr	$r \times 20\% \sin(t)$

Table 3: Simulation parameters of FD and NDO.

parameter	parameter perturbation
$\mathbf{R}_1$	[20, 20, 20]
$\mathbf{A}_1$	[5, 5, 5]
$\mathbf{A}_2$	[5, 5, 5]
$\mathbf{R}_2$	[8, 8, 8]
$\mathbf{A}_3$	[10, 10, 10]
$\mathbf{A}_4$	[3, 3, 3]

Case 1. Verify the performance of the controller based on BLF. Suppose the initial values of the attitude angles are $[\vartheta_0 \ \psi_0 \ \gamma_0]^T = [0^\circ \ 0^\circ \ 0^\circ]$ and $\mathbf{X}_{1d} = [\vartheta_r \ \psi_r \ \gamma_r]^T = [10^\circ \sin(5t) \ 10^\circ \sin(5t) \ 0^\circ]$. We can know that Z_1 satisfies $|Z_1| < K_{b_1}$. Simulation results are shown in Figures 4–9.

The attitude adjustment is divided into two stages, attitude adjustment stage and attitude keeping. From Figure 4, we can intuitively see that attitude controller based on BLF can make the attitude angles track desired attitude angles fast and accurately. During the attitude adjustment stage, the controller can constrain the attitude angle to the initial setting domain even though there are large interference errors in the three channels. In the attitude keeping stage, we can see that the tracking error of the pitch angle can stay within $\pm 0.2^\circ$ in most of the time and does not exceed $\pm 0.4^\circ$, the yaw angle tracking error does not exceed $\pm 0.5^\circ$, and the error of the roll angle does not exceed $\pm 0.2^\circ$. But, tracking accuracy of the yaw channel is the lowest and it is because the interference torque of is the largest. It can be seen from the simulation results that controller based on BLF can guarantee the tracking error in setting domain $(-K_{b_1}, K_{b_1})$ in the whole process and the attitude controller satisfies the requirement of fastness and accuracy.

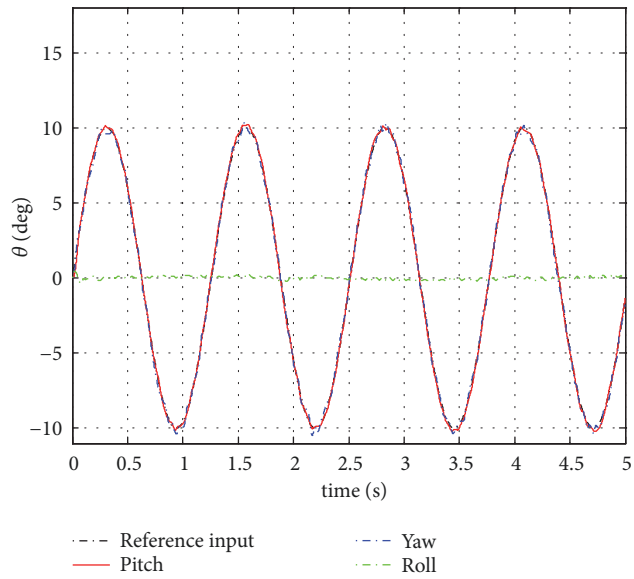

Figure 4: Attitude angle tracking curve.

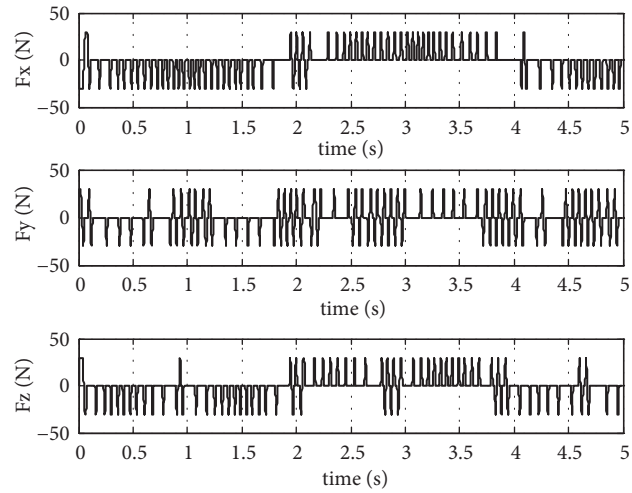

Figure 5: Thrust force curve.

As is shown in Figure 5, the thruster has a saturated working area and a large pulse in the initial stage of attitude control. When the thruster enters the duty cycle linear work area, the width of the thrust pulse also gradually decreases, which reflects the PSR modulator to adjust the width and frequency on the thrust. The simulation results show that the thruster starting frequency is low, KKV variable thrust attitude control accuracy and controller has a good performance. As showed in Figure 6, NDO has high approximation accuracy to unknown uncertainties and unknown time-varying disturbances and its estimation error is small. Accurate error estimation and compensation greatly improve the accuracy of attitude control.

Case 2. Verify the performance of the controller under strong interference conditions without estimation and compensation of uncertainties and disturbances. Initial values of the

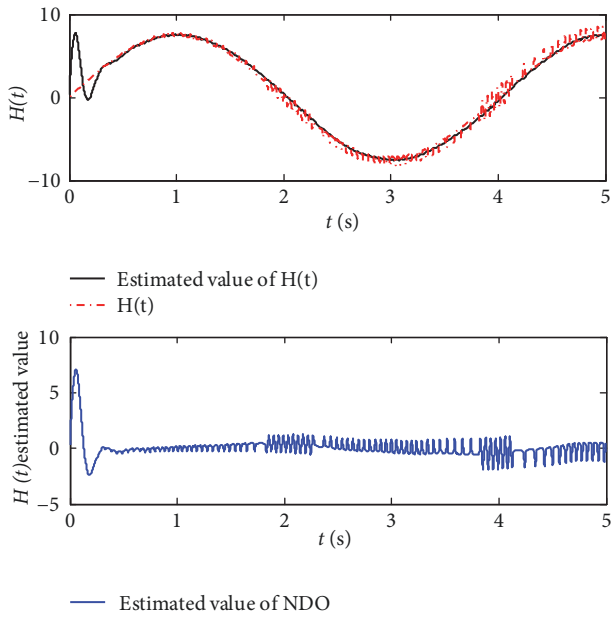

Figure 6: Estimated value and error of NDO.

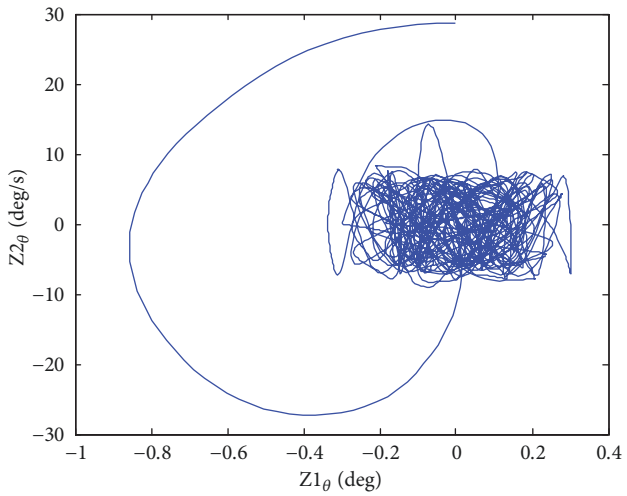

Figure 7: Pitch angle tracking error.

attitude angles and simulation settings are the same as Case 1. Simulation results are shown in Figures 10–13.

From Figures 11–13, we can know that the accuracy of controller obviously gets worse without estimation and compensation of uncertainties and disturbances. Pitch angle tracking error stays within ±0.5°, yaw angle tracking error stays within ±0.6°, and roll angle tracking error stays within ±0.4°. From Figure 10, we can know that the frequency of thruster switch is obviously increased, and it will cause more energy consumption. However, controller based on BLF can still guarantee the tracking error in setting domain $(-K_{b_1}, K_{b_1})$ in the whole process.

Case 3. Verify the performance of controller combining BLF with SMC and compared with the SMC. Suppose the initial values of the attitude angles are

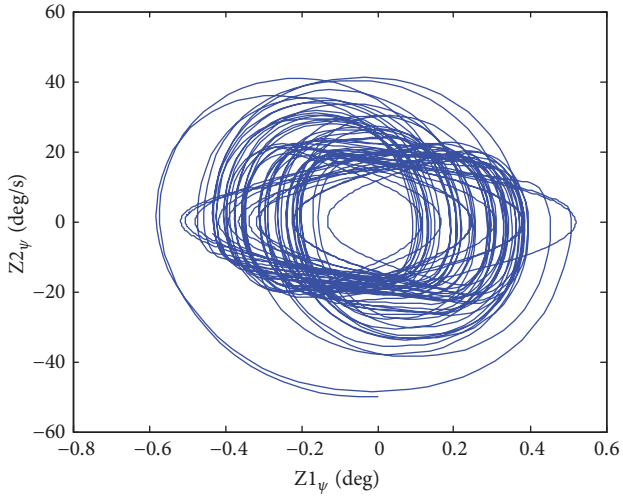

Figure 8: Yaw angle tracking error.

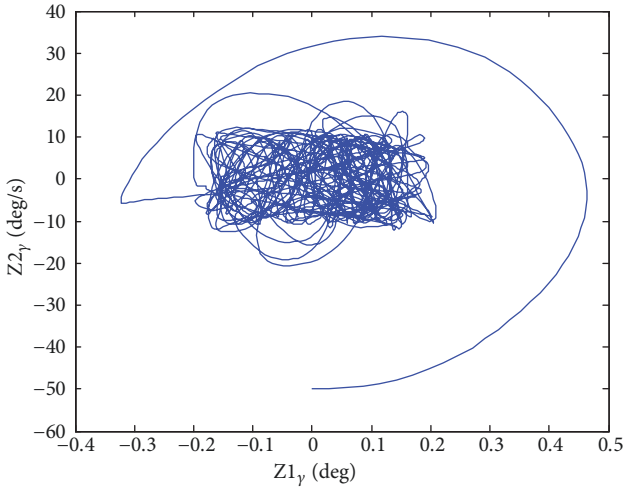

Figure 9: Roll angle tracking error.

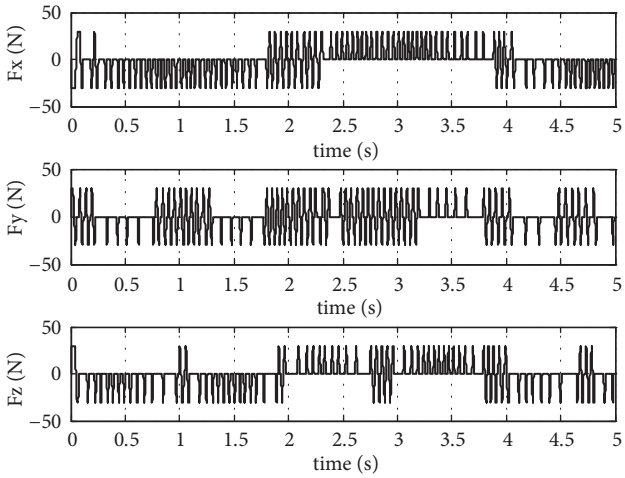

Figure 10: Thrust force curve.

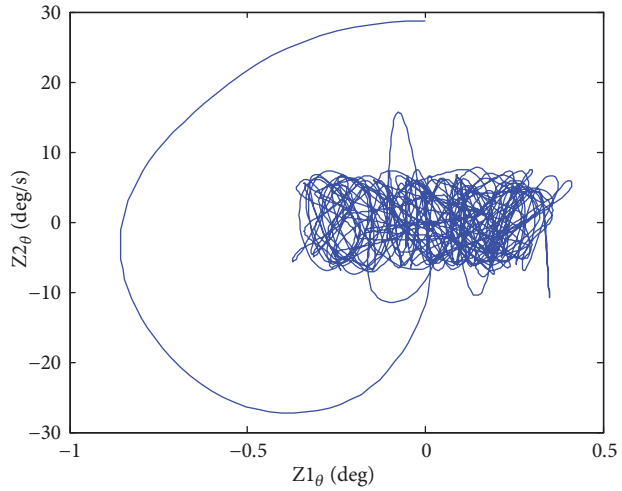

FIGURE 11: Pitch angle tracking error.

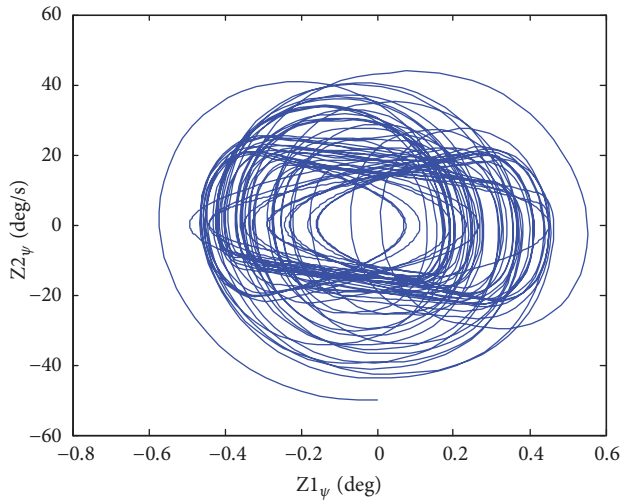

FIGURE 12: Yaw angle tracking error.

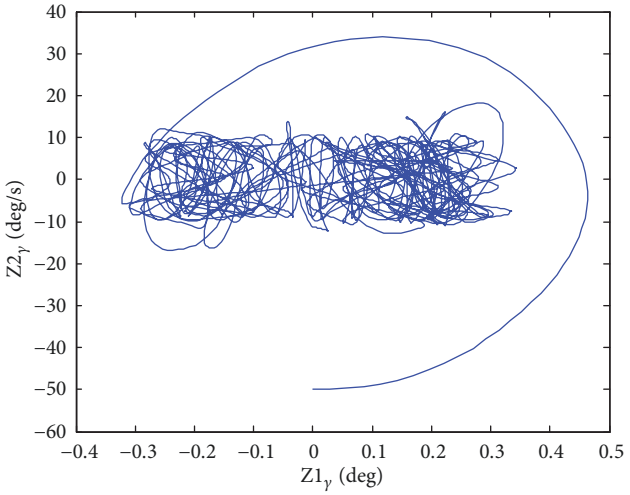

FIGURE 13: Roll angle tracking error.

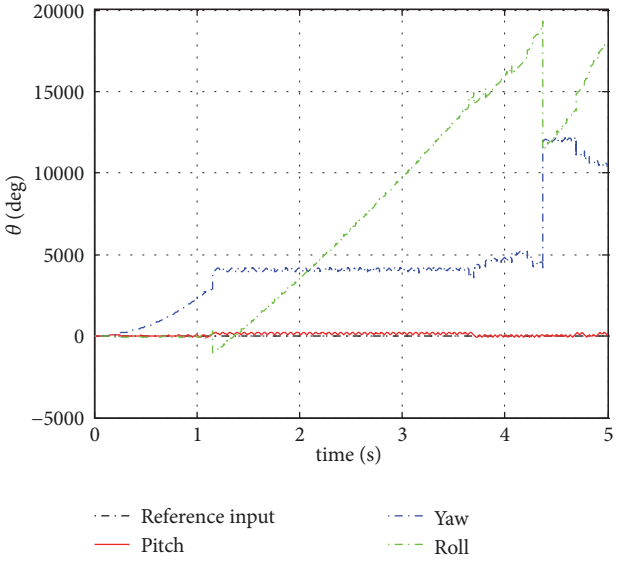

FIGURE 14: Attitude angle tracking curve with BLF controller.

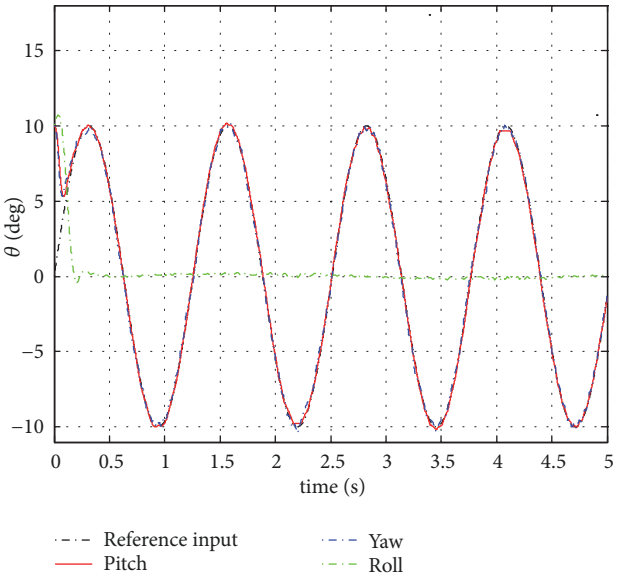

FIGURE 15: Attitude angle tracking curve combining BLF with SMC.

$[\vartheta_0 \ \psi_0 \ \gamma_0]^T = [10^\circ \ 10^\circ \ 10^\circ]$ and $X_{1d} = [\vartheta_r \ \psi_r \ \gamma_r]^T = [10^\circ \sin(5t) \ 10^\circ \sin(5t) \ 0^\circ]$. We can know that Z_1 does not satisfy $|Z_1| < K_{b_1}$. Simulation results are shown in Figures 14–23.

From Figure 14, we can know that when the initial error Z_1 does not satisfy $|Z_1| \leq K_{b_1}$, the BLF controller cannot guarantee the error global convergence. From Figures 17–19 we can know that the controller combining the SMC and BLF can guarantee the error global convergence. This is because when $|Z_1| > K_{b_1}$, mainly SMC is at work and it will make Z_1 converge to $(-K_{b_1}, K_{b_1})$, and then BLF controller is at work, and it will ensure the output constraint is not violated. From Figures 20–23, we can see that the SMC controller can guarantee a good steady performance, but

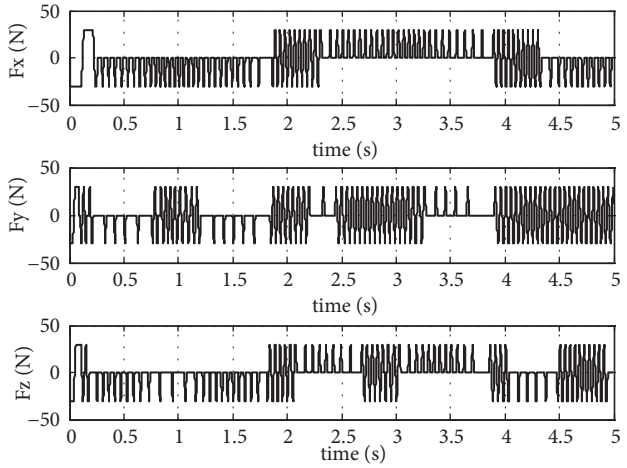

Figure 16: Thrust force curve.

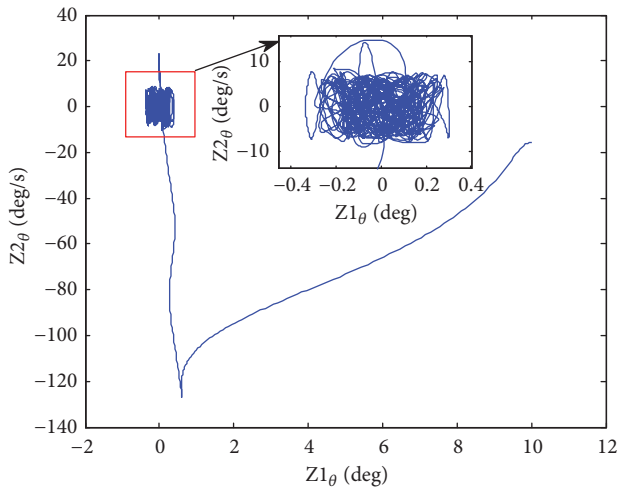

Figure 17: Pitch angle tracking error.

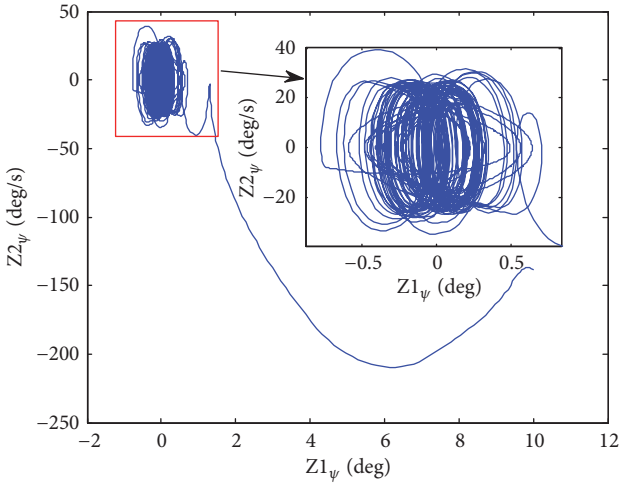

Figure 18: Yaw angle tracking error.

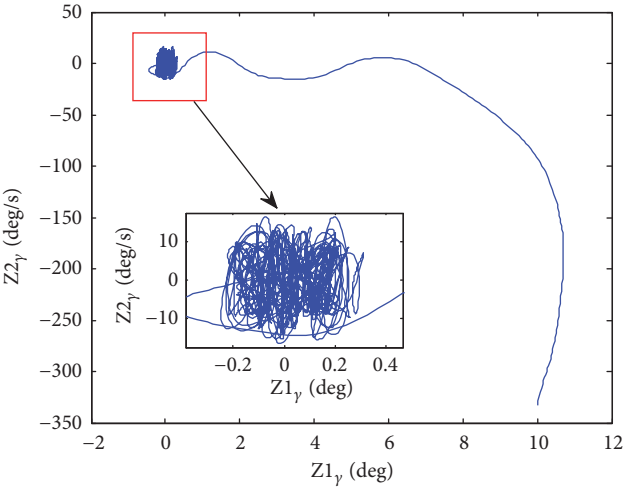

Figure 19: Roll angle tracking error.

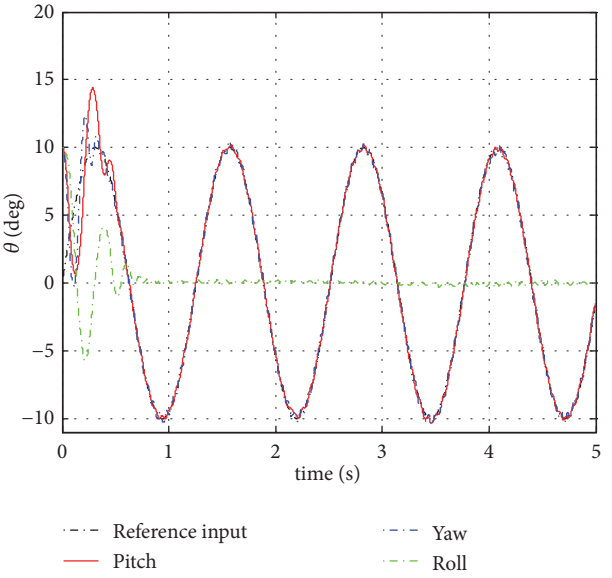

Figure 20: Attitude angle tracking curve with SMC controller.

its dynamic performance cannot be guaranteed. But the controller combining BLF with SMC has a good dynamic and steady performance.

Case 4. Verify the performance of PSR modulator. Compare the PSR modulator with the PWPF modulator. The range of optimal parameters for the PWPF and PSR is shown in Table II in [30]. The simulation parameters are selected as showed in Table 4, and the typical step signal is used as the reference signal. The PWPF and PSR modulator modulation curves are shown in Figure 24.

From Figure 24, we can know that the difference between the PSR modulator and the PWPF modulator is in the initial stage. The PSR modulator is turned on in the initial stage until the error is reduced to the shutdown threshold. However, the PWPF modulator is turned off in the initial stage until

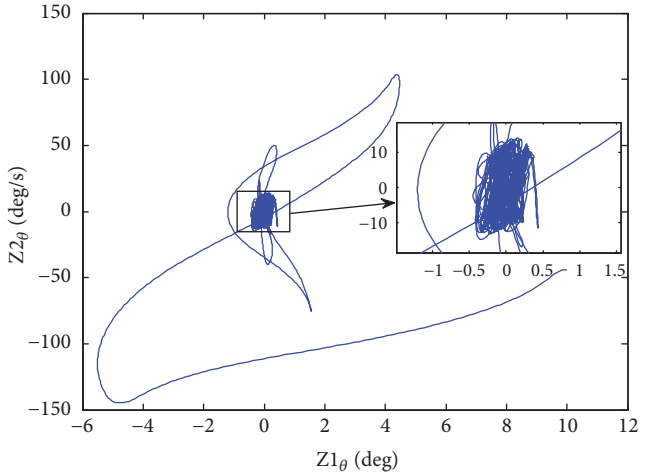

Figure 21: Pitch angle tracking error with SMC controller.

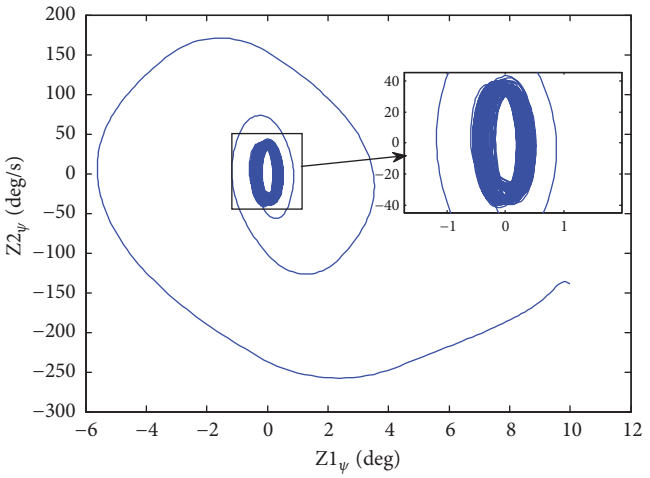

Figure 22: Yaw angle tracking error with SMC controller.

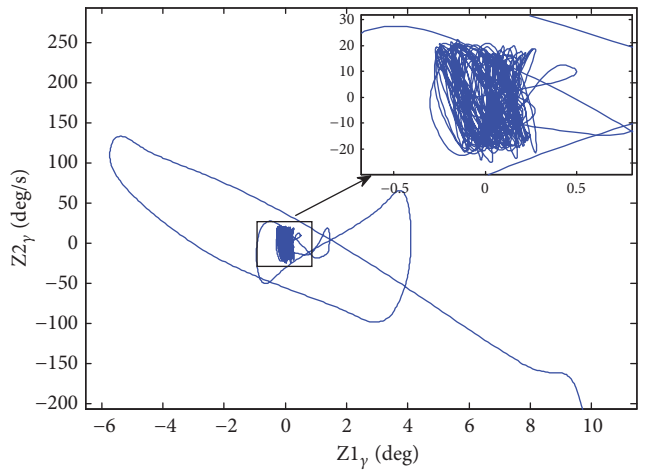

Figure 23: Roll angle tracking error with SMC controller.

Table 4: Modulator initial parameters.

PWPF	PSR
$K_m = 4$	$K_m = 2$
$T_m = 0.5$	$T_m = 0.3$
$U_{on} = 0.5$	$U_{on} = 0.45$
$U_{off} = 0.12$	$U_{off} = 0.3$

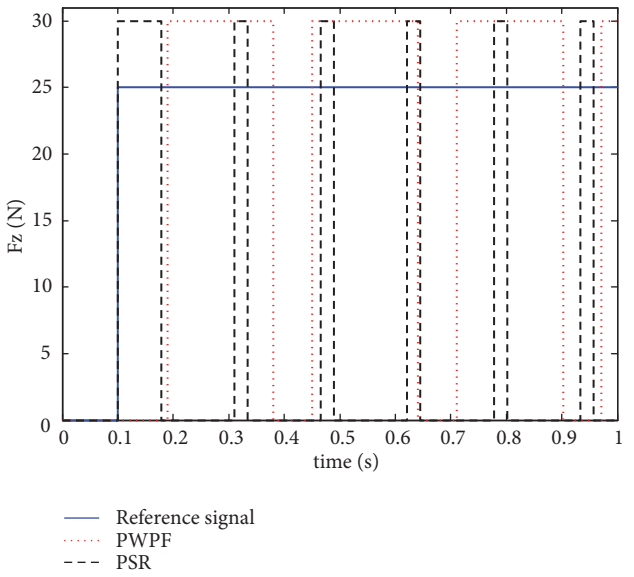

Figure 24: Modulators of PSR and PWPF response curves.

the error reaches the start-up threshold. This characteristic causes phase delay for PWPF modulator compared to the PSR modulator and may cause control system instability. At the same time, we clearly see from Figure 20 that the start-up time of the PWPF modulator is significantly longer than the PSR, which will lead to wasting fuel. Therefore, PSR modulator has obvious advantages compared with PWPF modulator.

5. Conclusion

In this paper, KKV attitude controller has been designed combining BLF with SMC to meet the state constraints caused by side window detection, and FD and NDO have been used to solve the problem of "differential explosion" and uncertainties estimation and compensation. Numerical simulations show that the designed controller can achieve attitude angles constraint and guarantee the error global convergence with fast convergence speed, high convergence accuracy and good robustness. NDO can achieve fast, smooth and accurate estimation of uncertainties, and unknown time-varying disturbances. PSR modulator can shape the continuous control command to pulse or on-off signals to meet the requirements of the thruster and achieve pseudo-linear operation. Meanwhile, it solved the PWPF modulator phase delay problem.

Data Availability

The data used to support the findings of this study are available from this paper.

Conflicts of Interest

The authors declare that they have no conflicts of interest.

Acknowledgments

This work was supported by the National Nature Science Foundation of China (nos. 61773398 and 61703421)

References

[1] Y. Yu, M. Hou, S. Zhang, and C. Yin, "A new adaptive proportional navigation based on side window detection," *Journal of Northwestern Polytechnical University*, vol. 34, no. 2, pp. 287–293, 2016.

[2] X. Xu and Y. Cai, "Pulse-width pulse-frequency based optimal controller design for kinetic kill vehicle attitude tracking control," *Applied Mathematics*, vol. 2, no. 25, pp. 565–574, 2011.

[3] J. Huang, H. Zhang, G. Li, and G. Tang, "Terminal guidance and control for kinetic kill vehicle adopting side window detection," in *Proceedings of the 7th IEEE Chinese Guidance, Navigation and Control Conference, CGNCC 2016*, pp. 363–368, Nanjing, China, August 2016.

[4] B. Q. Yang, T. Y. Zheng, S. L. Zhang et al., "Analysis and modeling of terminal guidance system for a flight vehicle with side-window detection," in *Proceedings of the Chinese Control Conference*, pp. 1051–1054, Nanjing, China, 2014.

[5] Y. Wang, J. Zhou, B. Zhao, and Y.-H. You, "Orbit control scheme of the terminal course of side window detection kinetic kill vehicle," *Journal of Solid Rocket Technology*, vol. 39, no. 4, pp. 588–593, 2016.

[6] T. Y. Zheng, Y. Yao, F. H. He et al., "Integrated guidance and control design of flight vehicle with side-window detection," *Chinese Journal of Aeronautics*, vol. 2, no. 3, p. 16, 2018.

[7] X. Wang, J. Guo, S. Tang, Q. Xu, Y. Ma, and Y. Zhang, "Robust nonsingular Terminal sliding mode backstepping control for air-breathing hypersonic vehicles," *Acta Aeronautica et Astronautica Sinica*, vol. 38, no. 3, pp. 3202871–32028713, 2017.

[8] M. Yue, L. J. Wang, and T. Ma, "Neural network based terminal sliding mode control for WMRs affected by an augmented ground friction with slippage effect," *IEEE/CAA Journal of Automatica Sinica*, vol. 4, no. 3, pp. 498–506, 2017.

[9] D. Ye, Y. Tu, and Z. Sun, "Sliding mode control for nonparallel-ground-track imaging using Chebyshev neural network," *Acta Aeronautica et Astronautica Sinica*, vol. 36, no. 9, pp. 3092–3104, 2015.

[10] Z. Zhu, Y. Xia, and M. Fu, "Attitude stabilization of rigid spacecraft with finite-time convergence," *International Journal of Robust and Nonlinear Control*, vol. 21, no. 6, pp. 686–702, 2011.

[11] X. Yang, X.-X. Yao, J. Zhang, and Y.-X. Liu, "Attitude tracking of KKV based on adaptive backstepping sliding mode control," *Journal of Solid Rocket Technology*, vol. 39, no. 5, pp. 715–722, 2016.

[12] T. Zhang, X. Shi, and Q. SHen, "Adaptive neural network dynamic surface control with unmodeled dynamics," *Control Theory & Applieation*, vol. 30, no. 4, pp. 475–482, 2013.

[13] M. Ran, Q. Wang, D. Hou, and C. Dong, "Backstepping design of missile guidance and control based on adaptive fuzzy sliding mode control," *Chinese Journal of Aeronautics*, vol. 27, no. 3, pp. 634–642, 2014.

[14] J. M. Bravo, D. Limon, T. Alamo, and E. F. Camacho, "On the computation of invariant sets for constrained nonlinear systems: an interval arithmetic approach," *Automatica*, vol. 41, no. 9, pp. 1583–1589, 2005.

[15] D. Limon, I. Alvarado, T. Alamo, and E. F. Camacho, "MPC for tracking piecewise constant references for constrained linear systems," *Automatica*, vol. 44, no. 9, pp. 2382–2387, 2008.

[16] T. Hatanaka and K. Takaba, "Computations of probabilistic output admissible set for uncertain constrained systems," *Systems Control and Information*, vol. 51, no. 11, pp. 499–512, 2007.

[17] G. Herrmann, M. C. Turner, and I. Postlethwaite, "A robust override scheme enforcing strict output constraints for a class of strictly proper systems," *Automatica*, vol. 44, no. 3, pp. 753–760, 2008.

[18] K. Kogiso and K. Hirata, "Reference governor for constrained systems with time-varying references," *Robotics and Autonomous Systems*, vol. 57, no. 3, pp. 289–295, 2009.

[19] K. B. Ngo, R. Mahony, and Z. Jiang, "Integrator backstepping using barrier functions for systems with multiple state constraints," in *Proceedings of the 44th IEEE Conference on Decision and Control, and the European Control Conference (CDC-ECC '05)*, pp. 8306–8312, Seville, Spain, December 2005.

[20] Y. Qiu, X. Liang, Z. Dai, J. Cao, and Y. Chen, "Backstepping dynamic surface control for a class of non-linear systems with time-varying output constraints," *IET Control Theory & Applications*, vol. 9, no. 15, pp. 2312–2319, 2015.

[21] B. Niu and J. Zhao, "Tracking control for output-constrained nonlinear switched systems with a barrier Lyapunov function," *International Journal of Systems Science*, vol. 44, no. 5, pp. 978–985, 2013.

[22] Y.-J. Liu and S. Tong, "Barrier Lyapunov functions-based adaptive control for a class of nonlinear pure-feedback systems with full state constraints," *Automatica*, vol. 64, pp. 70–75, 2016.

[23] K. P. Tee, S. S. Ge, and E. H. Tay, "Barrier Lyapunov functions for the control of output-constrained nonlinear systems," *Automatica*, vol. 45, no. 4, pp. 918–927, 2009.

[24] K. P. Tee, B. Ren, and S. S. Ge, "Control of nonlinear systems with time-varying output constraints," *Automatica*, vol. 47, no. 11, pp. 2511–2516, 2011.

[25] W. Sun, J. Lan, and J. T. W. Yeow, "Constraint adaptive output regulation of output feedback systems with application to electrostatic torsional micromirror," *International Journal of Robust and Nonlinear Control*, vol. 25, no. 4, pp. 504–520, 2015.

[26] W. He, S. Zhang, and S. S. Ge, "Adaptive control of a flexible crane system with the boundary output constraint," *IEEE Transactions on Industrial Electronics*, vol. 61, no. 8, pp. 4126–4133, 2014.

[27] F. Yan and J. Wang, "Fuel-assisted in-cylinder oxygen fraction transient trajectory shaping control for diesel engine combustion mode switching," in *Proceedings of the 2011 American Control Conference, ACC 2011*, pp. 1573–1578, San Francisco, Calif, USA, July 2011.

[28] D. Meijun, D. Zhou, and C Dalian, "Research of terminal guidance law and PWPF modulator for near space interceptor based on finite time theory," *Acta Aeronautica et Astronautica Sinica*, vol. 38, no. 25, pp. 341481–341483, 2017.

[29] Q. Wang, B.-Q. Yang, and K.-M. Ma, "PWPF optimizing design and its application research to terminal guidance of Kinetic killing vehicle," *Yuhang Xuebao/Journal of Astronautics*, vol. 26, no. 5, pp. 576–580, 2005.

[30] M. Navabi and H. Rangraz, "Comparing optimum operation of Pulse Width-Pulse Frequency and Pseudo-Rate modulators in spacecraft attitude control subsystem employing thruster," in *Proceedings of the 6th International Conference on Recent Advances in Space Technologies, RAST 2013*, pp. 625–630, Istanbul, Turkey, June 2013.

[31] Y. Tang, Y. Wu, M. Wu, X. Hu, and L. Shen, "Nonlinear tracking-differentiator for velocity determination using carrier phase measurements," *IEEE Journal of Selected Topics in Signal Processing*, vol. 3, no. 4, pp. 716–725, 2009.

[32] B. Q. Yang, *Research on guidance and control law for exo-atmospheric KKV based on predictive control [Ph. D. thesis]*, Harbin Institute of Technology, Harbin, China, 2009.